Biomedical Signal Processing and Control 27 (2016) 134–144

Contents lists available at ScienceDirect

Biomedical Signal Processing and Control

journal homepage: www.elsevier.com/locate/bspc

A revised scheme for real time ECG Signal denoising based on recursive filtering

S. Cuomo [a,*], G. De Pietro [b], R. Farina [b], A. Galletti [c], G. Sannino [b]

[a] Department of Mathematics and Applications, University of Naples Federico II, Via Cinthia, Naples 80126, Italy
[b] Institute for High-Performance Computing and Networking, National Research Council (ICAR-CNR), Via Pietro Castellino 111, Naples 80131, Italy
[c] University of Naples Parthenope, Department of Science and Technology, Naples, Italy

ARTICLE INFO

Article history:
Received 22 July 2015
Received in revised form
10 December 2015
Accepted 19 February 2016
Available online 15 March 2016

Keywords:
Electrocardiogram
Real time signal denoising
Recursive filters
Rational polynomial approximation
Boundary conditions

ABSTRACT

In many healthcare applications, artifacts mask or corrupt important features of Electrocardiogram (ECG) signals. In this paper we describe a revised scheme for ECG signal denoising based on a recursive filtering methodology. We suggest a suitable class of kernel functions in order to remove artifacts in the ECG signal, starting from noise frequencies in the Fourier domain. Our approach does not require high computational requirements and this feature offers the possibility of an implementation of the scheme directly on mobile computing devices. The proposed scheme allows local denoising and hence a real time visualization of the signal by means of a strategy based on boundary conditions. Experiments on real datasets have been carried out in order to test, in terms of computation and accuracy, the proposed algorithm. Finally, comparative results with other well-known denoising methods are shown.

1. Introduction

The Electrocardiogram (ECG) signal is one of the most important tools for the detection of cardiovascular diseases. It is a graphical representation of cardiac activity and it provides significant information about the functional conditions of the heart and the circulatory system. Due to the importance of the ECG signal and the related heart rate variability measurements (e.g. [1]) in the diagnosis of serious episodes, like myocardial ischemia or atrial fibrillation, the denoising signal process has become a very significant task in the medical and engineering communities [2]. Generally, the recorded signal could be corrupted by various kinds of noise signal, as discussed in [3], namely artifacts, of which the most common are well highlighted in [4]. They include power line interference, electrode contact noise, motion artifacts, muscle contraction interference, baseline drift, and some instrumental noise generated by the electronic ECG monitoring device, all of which can corrupt the ECG and lead to a wrong diagnosis. Ref. [5] studied the effects of baseline drift and power line interference on the ability of the technique to detect the morphology of some signal quality features. Several methods have been applied to model and to denoise the ECG signal, such as band pass filters (e.g. [6]), adaptive filters (e.g. [7]), the ensemble averaging technique (e.g. [8]), extended Kalman filters (e.g. [9]), Wiener filtering (e.g. [10]), Empirical Mode Decomposition (e.g. [11]), and wavelet denoising (e.g. [12]). For other methods see [13]. Although some of these methods have demonstrated a good performance in terms of Signal to Noise Ratio (SNR), they can be sensitive to varying parameters. Moreover, in ECG filtering, a crucial problem is the preservation of the shape, which is achieved by several algorithms, for example by non-local means filtering, as in [14]. These methodologies belong to the *off-line methods*, where the electrical data are first recorded and then a denoising algorithm is applied to improve the quality of the acquired signal. This approach represents a strong limitation in several contexts, for example in healthcare systems that are undergoing a transformation, as documented in [15]. Moreover, when the ECG recordings are provided by wearable sensors, that transmit data to a mobile device using wired or wireless communication, it is necessary to display and to process healthcare and biomedical information in a real time scenario. For this applicative health care context, new approaches based on novel algorithms and smart software frameworks have been widely explored to improve electronic health care (e-health) services, especially for the acquisition and filtering of biomedical signals [16–18]. In *real time signal processing*, two new aspects are required: the computational efficiency of the

* Corresponding author.
E-mail addresses: salvatore.cuomo@unina.it (S. Cuomo), giuseppe.depietro@na.icar.cnr.it (G. De Pietro), raffaele.farina@na.icar.cnr.it (R. Farina), ardelio.galletti@uniparthenope.it (A. Galletti), giovanna.sannino@na.icar.cnr.it (G. Sannino).

http://dx.doi.org/10.1016/j.bspc.2016.02.007
1746-8094/

algorithm and the ability to process a signal in a local way. This is especially true for wearable sensors that send only a few samples of the signal (usually equivalent to a quarter of a second) in a data packet format to a mobile device. Here the computing device should first process the actual part of the received signal and then switch in the next data packets. In this paper, starting from a methodology based on recursive filtering, applied successfully in another research field, such as by [19–24], we propose a revised numerical scheme for real time ECG denoising [25], with a low computational requirement, in terms of memory and time consumption. We are interested in the removal of base line drift, power line interference and, in general, of every noise in which the frequency spectrum wanders within a known and limited range. A first version of the scheme was presented in [26]. In this paper, we describe in detail the procedure to derive the filtering coefficients which depends on the frequency range of the considered noise. Moreover, we provide suitable boundary conditions that allow the scheme to realize the signal filtering in a local way and the visualization of the data in real time directly on the mobile device. The proposed approach is based on the analysis of the signal in the Fourier domain, but it does not require a direct application of the (Fast) Fourier Transform. This feature makes our algorithm suitable for direct implementation in mobile applications or wearable sensors without the use of any library for scientific computing. Finally, in this paper we compare the proposed algorithm with other known methods, especially in terms of quality measurements and computational aspects.

The paper is organized as follows: in Section 2 we report some preliminary mathematical considerations; Section 3 is devoted to the derivation of the numerical scheme; in Section 4 we provide a scheme implementation for real time denoising and compare it with other known algorithms for denoising and, finally, we draw some conclusions in Section 5.

2. Mathematical background

In this section, we present the preliminary mathematical considerations in order to derive a numerical scheme for the denoising of an ECG signal. Let s_0 denote a real function such that:

$$s_0 = s + \epsilon$$

with s the original signal and ϵ a noise function. As in [27] the denoising process can be viewed as a convolution of s_0 with a function h, Lebesgue integrable, i.e.:

$$s_h(t) = h(x) \otimes s_0(x) = \int_{-\infty}^{+\infty} h(t-x)s_0(x)\,dx, \quad \forall t \in \mathbb{R}. \tag{1}$$

In this work, to determine a suitable convolution kernel h, we use the following mathematical tools (e.g. [28]):

- the Fourier Transform $\mathcal{F}$ of a signal f:

$$F(\omega) = \mathcal{F}(f)(\omega) = \frac{1}{\sqrt{2\pi}} \int_{-\infty}^{+\infty} f(x)e^{-i\omega x}\,dx, \quad \forall \omega \in \mathbb{R}; \tag{2}$$

- the Fourier anti-Transform $\mathcal{F}^{-1}$ of F:

$$f(t) = \mathcal{F}^{-1}(F)(t) = \frac{1}{\sqrt{2\pi}} \int_{-\infty}^{+\infty} F(x)e^{itx}\,dx, \quad \forall t \in \mathbb{R}; \tag{3}$$

- the convolution theorem:

$$\mathcal{F}(h \otimes f) = \mathcal{F}(h) \cdot \mathcal{F}(F) = H \cdot F; \tag{4}$$

- the Plancherel theorem:

$$\int_{-\infty}^{\infty} |f(x)|^2\,dx = \int_{-\infty}^{\infty} |F(\omega)|^2 d\omega. \tag{5}$$

The main idea of this work is to find a convolution kernel h, to denoise s_0, starting from its Fourier Transform $H = \mathcal{F}(h)$. Now, let us suppose that:

$$S_h = \mathcal{F}(s_h), \quad S_0 = \mathcal{F}(s_0), \quad S = \mathcal{F}(s) \quad \text{and} \quad \mathcal{E} = \mathcal{F}(\epsilon).$$

If we assume that the Fourier Transform $H = \mathcal{F}(h)$ of h is such that:

$$\begin{cases} H \cdot S = S, \\ H \cdot \mathcal{E} = 0, \end{cases} \tag{6}$$

then, it can be easily proved, by exploiting the Fourier Transform, Convolution Theorem and Fourier anti-Transform, that:

$$s_h = h \otimes s_0 = \mathcal{F}^{-1}(H \cdot S_0) = \mathcal{F}^{-1}(H \cdot S + H \cdot \mathcal{E}) = \mathcal{F}^{-1}(H \cdot S) = s. \tag{7}$$

Observing that if the original and noise signals, s and ϵ, have the property:

$$supp\, S \cap supp\, \mathcal{E} = \emptyset \tag{8}$$

then, it is sufficient to take the following function H, that satisfies the condition (6):

$$H(\omega) = \begin{cases} 0 & \forall\ \omega \in\ supp\, \mathcal{E}, \\ 1 & \text{otherwise.} \end{cases} \tag{9}$$

Then, in these hypotheses, the original signal s can be completely restored by the convolution in (7). Nevertheless, a satisfying solution s_h (an approximation of s) can be achieved also when the measure of the set $supp\, S \cap supp\, \mathcal{E}$ can be considered quite small (e.g. [29]). However, the mathematical form of H in (9), with its discontinuities, prevents us from determining the numerical scheme. Therefore, for our purpose, as we will show in the next section, instead of H, we will use another function $\tilde{H}$, a rational polynomial, which emulates the properties of H. In the next section we will adapt the standard methodology on recursive filtering, which is based on the Infinite Impulse Response (IIR) Gaussian recursive filter of [19,20,23,24,30], with the aim of deriving an efficient numerical scheme for the denoising of the ECG signal in real time.

3. The proposed scheme

In this section we derive a numerical scheme for ECG denosing. In the first discussion, we suggest a suitable kernel function adopted to select some frequencies in the Fourier domain. In the second subsection, we use the recursive filtering theory to obtain an algorithm for the denoising of an ECG signal. In this work, we have supposed the set of the frequencies ($supp\, \mathcal{E}$) of the noise ϵ to be included in an interval $[\mu - \sigma, \mu + \sigma]$ with μ and $\sigma > 0$.

3.1. The Kernel function $\tilde{H}(\omega)$

The main idea, here, is to determine a suitable kernel function $\tilde{H}$ fixing its behavior in the Fourier domain. The step function H (see the continuous line in Fig. 1) is the ideal function to cut off the nonzero values on the noise frequencies and keep unchanged the nonzero values on the original signal's frequencies. However, due to its discontinuities, here it is used a function with a Gaussian like shape (see [19,30]) as for example the function G (the dash-dot line in Fig. 1):

$$G(\omega) = 1 - e^{-\frac{(\omega-\mu)^2}{2\sigma^2}}, \quad \forall \omega \in \mathbb{R}. \tag{10}$$

In particular, we have used the function $\tilde{H}$ (see the dashed line in Fig. 1) defined as:

$$\tilde{H}(\omega) = \frac{(\omega-\mu)^2}{2\sigma^2 + (\omega-\mu)^2}, \quad \forall \omega \in \mathbb{R}. \tag{11}$$

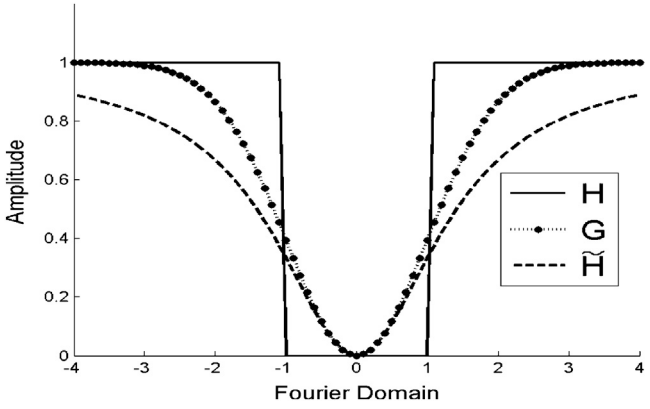

Fig. 1. H, $\tilde{H}$ and G functions with $\mu = 0$ and $\sigma = 1$.

The function in (11) is a rational approximation of the function G, obtained by taking the first two terms in the Taylor expansion of the following exponential function:

$$e^{\frac{(\omega-\mu)^2}{2\sigma^2}} = \sum_{i=0}^{+\infty} \frac{1}{i!} \left(\frac{(\omega-\mu)^2}{2\sigma^2} \right)^i. \tag{12}$$

The properties of the functions $\tilde{H}$ and G are given in the following proposition:

Proposition 3.1. *For the $\tilde{H}$ and G functions, the following properties hold:*

1. $0 \le G(\omega), \tilde{H}(\omega) < 1, \quad \forall \omega \in \mathbb{R}$;
2. $\tilde{H}(\mu) = G(\mu) = 0$;
3. $\lim_{\omega \to \pm\infty} \tilde{H}(\omega) = \lim_{\omega \to \pm\infty} G(\omega) = 1$;
4. $\tilde{H}(\omega)$ *and* $G(\omega)$ *are symmetrical with respect to the axis* $\omega = \mu$;
5. $\tilde{H}(\mu \pm \sigma) = 1/3$;
6. $\tilde{H}(\omega) = \tilde{H}_l(\omega) \cdot \tilde{H}_r(\omega), \quad \forall \omega \in \mathbb{R}$, *where we set:*

$$\tilde{H}_l(\omega) = \frac{i\omega - i\mu}{i\omega + (\sqrt{2}\sigma - i\mu)}, \qquad \tilde{H}_r(\omega) = \frac{-i\omega + i\mu}{-i\omega + (\sqrt{2}\sigma + i\mu)}. \tag{13}$$

The choice of function $\tilde{H}$ in (11) can still remove the noisy ϵ, even if its frequency spectrum is wandering in the interval $[\mu - \sigma, \mu + \sigma]$. To proof this feature, now we give an upper bound of distance between s_h and $s_{\tilde{h}}$ in the 2 norm:

$$\|s_h - s_{\tilde{h}}\|_2 = \left(\int_{-\infty}^{\infty} (s_h(x) - s_{\tilde{h}}(x))^2 \, dx \right)^{(1/2)}, \tag{14}$$

which only depends on the parameter σ.

Proposition 3.2. *Let H be as in (9), $\tilde{H}$ as in (11), $s_h = h \otimes s_0$, with $h = \mathcal{F}^{-1}(H)$ and $s_{\tilde{h}} = \tilde{h} \otimes s_0$, with $\tilde{h} = \mathcal{F}^{-1}(\tilde{H})$. An upper bound of the distance between the signals s_h and $s_{\tilde{h}}$ is given by the following inequality:*

$$\|s_h - s_{\tilde{h}}\|_2 < \mathcal{O}(\sqrt{\sigma}) \|s_0\|_2. \tag{15}$$

Proof. The proof is shown in Appendix A.□

The upper bound in (15) shows that, for small values of σ, $s_{\tilde{h}}$ can be viewed as a reliable approximation of s_h, regardless of the choice of μ.

3.2. The revised recursive filtering scheme

Starting from [19,20,23,24,30] we reduce the effects of the additive noise function ϵ on the original signal s, when *supp* $\mathcal{E} \subset [\mu - \sigma, \mu + \sigma]$. As a preliminary remark, we observe that if $\tilde{h} = \mathcal{F}^{-1}(\tilde{H})$, with $\tilde{H}$ as in (11), then for the function $s_{\tilde{h}} = \tilde{h} \otimes s_0$ it holds that:

$$s_{\tilde{h}} = \mathcal{F}^{-1}(\tilde{H} \cdot S_0) = \mathcal{F}^{-1}(\tilde{H}_l \cdot \tilde{H}_r \cdot \cdot S_0) = \tilde{h}_l \otimes (\tilde{h}_r \otimes s_0), \tag{16}$$

where the functions $\tilde{h}_l$ and $\tilde{h}_r$ are defined as:

$$\tilde{h}_l = \mathcal{F}^{-1}(\tilde{H}_l) \quad \text{and} \quad \tilde{h}_r = \mathcal{F}^{-1}(\tilde{H}_r),$$

with $\tilde{h}_l$ and $\tilde{h}_r$ as in (13). Now we introduce the discrete signals:

$$\vec{s}_0 = (s_0[j])_{j \in \mathbb{Z}}, \quad \vec{s} = (s[j])_{j \in \mathbb{Z}} \quad \text{and} \quad \vec{s}_{\tilde{h}} = (s_{\tilde{h}}[j])_{j \in \mathbb{Z}},$$

which are obtained from the continuous signals $s_0, s, s_{\tilde{h}}$ considering only their values on a infinite grid with a stepsize τ. The discrete signals have the following form:

$$s_0[j] = s_0(j\tau), \qquad s[j] = s(j\tau), \qquad s_{\tilde{h}}[j] = s_{\tilde{h}}(j\tau), \quad j = -\infty, \ldots, +\infty. \tag{17}$$

Now, given $\vec{s}_0$, we look for a fast method for computing $\vec{s}_{\tilde{h}}$ given $\vec{s}_0$. The scheme is obtained by means of the discretization of the continuous scheme:

$$\mathcal{S}_{\tilde{h}} = \tilde{H}_l \cdot \tilde{H}_r \cdot S_0, \tag{18}$$

where $\tilde{h}_l$ and $\tilde{h}_r$ in (13) represent respectively cause and anti-cause stable differential equations for continuous signals that can be transformed into causal and anti-causal difference equations for discrete signals by means of standard techniques (e.g. [28]). The classic methods for discretization are bilinear transform, finite differences, zero-pole matching method and others (e.g. [28]).

For our scheme we use the zero-pole matching method (ZPM); this approach has the advantage of transforming stable differential equations into stable difference equations. It works in the following way; given a polynomial such as:

$$p(s) = s + (a + ib), \quad s \in \mathbb{C}; \tag{19}$$

the zero-pole matching method exploits the following position:

$$z = e^{s\tau}. \tag{20}$$

Using Eq. (20), the zero of $p(s)$ is transformed from a point lying in the s-plane into a point in the z-plane. This new point is later used to build the polynomial in the z variable, by posing:

$$z = e^{-(a+ib)\tau} \Leftrightarrow z - e^{-(a+ib)} = 0. \tag{21}$$

Finally, by multiplying the right hand side of (21) to $z - e^{-(a-ib)}$, we obtain the following z polynomial:

$$p(z) = e^{-2a\tau} - 2e^{-a\tau} \cos(b\tau) z + z^2. \tag{22}$$

In the next proposition, starting from the zeros and poles (Table 1) of H_l and H_r in (13), we obtain our scheme. for the computing of $\vec{s}_{\tilde{h}}$ given $\vec{s}_0$

Theorem 3.3. *Let $\vec{s}_0, \vec{s}_{\tilde{h}}$ be discrete signals with the sampling step τ. Then, the denoised discrete signal $\vec{s}_{\tilde{h}}$ can be obtained from the noisy discrete signal $\vec{s}_0$ by means of the following forward and backward numerical scheme:*

Table 1
Zeros and poles of $\tilde{H}_l(\omega)$ and $\tilde{H}_r(\omega)$.

H_l/H_r	Zeros	Poles
$H_l(\omega)$	$i\mu$	$-\sqrt{2}\sigma + i\mu$
$H_r(\omega)$	$i\mu$	$\sqrt{2}\sigma + i\mu$

$$p_{\tilde{h}}[j] = b_0 s_0[j] + b_1 s_0[j-1] + b_2 s_0[j-2] + a_1 p_{\tilde{h}}[j-1] + a_2 p_{\tilde{h}}[j-2], \quad j = -\infty, \ldots, +\infty, \tag{23}$$

$$s_{\tilde{h}}[j] = b_0 p_{\tilde{h}}[j] + b_1 p_{\tilde{h}}[j+1] + b_2 p_{\tilde{h}}[j+2] + a_1 s_{\tilde{h}}[j+1] + a_2 s_{\tilde{h}}[j+2], \quad j = +\infty, \ldots, -\infty, \tag{24}$$

where the recursive scheme coefficients in (23) and (24) are:

$$b_0 = 1, \quad b_1 = -2\cos(\mu\tau), \quad b_2 = 1 \tag{25}$$

and

$$a_1 = 2e^{-\sqrt{2}\sigma\tau}\cos(\mu\tau), \quad a_2 = -e^{-2\cdot\sqrt{2}\sigma\tau}. \tag{26}$$

Proof. The proof is shown in Appendix A. □

Eqs. (23) and (24) are conveniently referred to as the advancing and backing filters, respectively, since in the former the index j must be treated as in increasing order while, in the latter, it must be treated in decreasing order (see [30]). The advancing processing in (23) derives from the H_r function in (13): setting $-s = -i\omega$ and exploiting Eq. (20), the ZPM method and the theorem of delay [28], we derive a forward scheme for the $p_{\tilde{h}}[j]$ values. In the same way, posing $s = i\omega$, we obtain from the H_l function in (13) the backing processing in (24). The forward and backward schemes in (23) and (24) are necessary to achieve the stability in the filtering algorithm (see [19,28]). More details on the derivation of the filtering scheme are given in the proof of Theorem 3.3 in Appendix A. Now, if we assume that the support of the input signal $\vec{s}_0$ is in the grid $\{1, 2, \ldots, n\}$, then Eqs. (23) and (24) can be implemented in an algorithm in which the index j increases from 1 to n, for the advancing filter, and decreases from n to 1, for the backing filter. This scheme needs to prime the advancing filter, by setting the values $p_{\tilde{h}}[j]$, for $j \in \{0, -1, \ldots, 1-N\}$, and the advancing filter, by setting the values $s_{\tilde{h}}[j]$ for $j \in \{n+1, n+2, \ldots, n+N\}$. For example, a common choice is to set to zero the required $p_{\tilde{h}}[j]$ and $s_{\tilde{h}}[j]$ values, i.e.:

$$\begin{aligned} &p_{\tilde{h}}[-N+1] = p_{\tilde{h}}[-N+2] = \ldots = p_{\tilde{h}}[0] = 0; \\ &s_{\tilde{h}}[n+1] = s_{\tilde{h}}[n+2] = \ldots = s_{\tilde{h}}[n+N] = 0. \end{aligned} \tag{27}$$

However, this assumption gives rise to a well-known edge effect, already noticed in [31], and discussed in detail in [21,22]. An outline of such a scheme, implementing (23), (24) and (27), is provided in Algorithm 1.

Algorithm 1. Filtering scheme

Input: s_0, μ, σ **Output:** $s_{\tilde{h}}$

set b_0, b_1, b_2, a_1, a_2 % scheme coefficients precomputation
for $j = 1, 2, \ldots, N$ % left zero end conditions
  $p_{\tilde{h}}[j-N] := 0$
endfor
for $j = 1, 2, \ldots, n$ % advancing process
  $p_{\tilde{h}}[j] = b_0 s_0[j] + b_1 s_0[j-1] + b_2 s_0[j-2] + a_1 p_{\tilde{h}}[j-1] + a_2 p_{\tilde{h}}[j-2]$
endfor
for $j = 1, 2, \ldots, N$ % right zero end conditions
  $s_{\tilde{h}}[n+j] := 0$
endfor
for $j = n, \ldots, 1$ % backing process
  $s_{\tilde{h}}[j] = b_0 p_{\tilde{h}}[j] + b_1 p_{\tilde{h}}[j+1] + b_2 p_{\tilde{h}}[j+2] + a_1 s_{\tilde{h}}[j+1] + a_2 s_{\tilde{h}}[j+2]$
endfor

4. Scheme implementation and performance results

In this section, we discuss, some implementation details and performance results, in terms of the accuracy of the denoising and the efficiency, for the scheme presented in Theorem 3.3. In the first subsection we focus on the boundary conditions, that guarantee the local computation, in other words ensure the processing of the ECG data in real time. In the second subsection, we report the performance metrics.

4.1. Boundary conditions and implementation details

We have implemented a system framework for real time ECG denoising and visualization. In the denoising module of the system, for the pre-processing of the ECG data we can choose different denoising algorithms for the removal of the main artifacts on the ECGs such as power line interference, base line drift and other noises. In our system we have used as ECG device the Zephyr BioHarness BH3, an advanced physiological monitoring device in which the data are transmitted by means of Bluetooth technology. It is small in size and provides a medical-grade ECG, heart rate, breathing rate, and 3-axis accelerometery. The monitor can be used with the BioHarness strap, a lightweight elasticized component that incorporates Zephyr Smart Fabric ECG and breathing rate sensors. The heart rate (HR) data are captured through electrode sensors housed within the chest strap (i.e. detecting R wave forms) sampled at 250 Hz and reported as beats per minute (br min^{-1}). Bluetooth-based data transmission allows the monitoring of physiological data by using any mobile device with Bluetooth technology, such as a laptop, phone or PDA. An example of the system framework is shown in Fig. 2.

The numerical scheme, derived in Theorem 3.3, is the core of the software framework. All the denoising modules are obtained by Eqs. (23) and (24), setting suitably the range $[\mu-\sigma, \mu+\sigma]$ of the noise frequencies to cut off. The scheme works directly on the computing devices that are for example smartphones or tablets. In real applications, this is applied to a signal $\vec{s}_0$ with a bounded domain and not to a signal with an unbounded domain, as stated in Theorem 3.3. The proposed algorithm belongs to the family of recursive filters, that suffer from the transition between the forward and the backward procedures as is well-known in recursive filter theory (see [31]). In fact, the forward and backward processes only give the correct result when the full double recursion is run without any truncation, i.e. when we process signals with an infinite size. Ref. [22] studied in depth the effects of these errors on the Gaussian convolution of a generic signal, with compact support, by means of our recursive filter. In particular, the authors proposed a way of minimizing the effects of truncation on the solution, extending in a smart way the domain of the signal with respect to the number of iterations of the filter. Then, in the case of signals with a compact support, after the forward procedure (23), we need optimal initial conditions for the backward procedure in (24). An incorrect truncation can produce significant amplitude and distortion for all points close to the boundaries also called edge effects. This problem prevents our scheme the filtering and visualization of the denoised signal, in real time, during a long ECG recording. In Fig. 3, we show the results of the software framework, based on our scheme without boundary conditions, which acquires and filters an ECG signal (with a sampling frequency of 250 Hz) each 0.25 s. Fig. 3 shows that the recursive scheme, without turning conditions, can produce distortions on the signal (marked in yellow in the figure), often

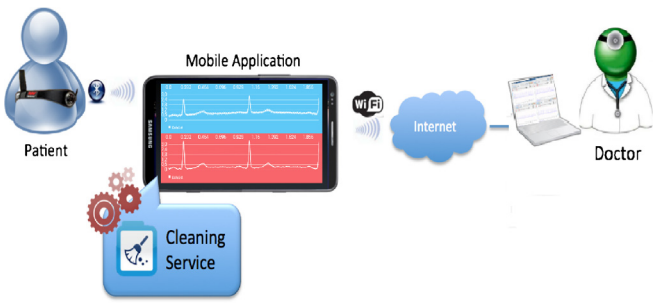

Fig. 2. Example of a software framework for mobile computing, that records an ECG with a wearable sensor and processes the signal by means of the proposed scheme. Subsequently the results are sent to the remote server of the doctor.

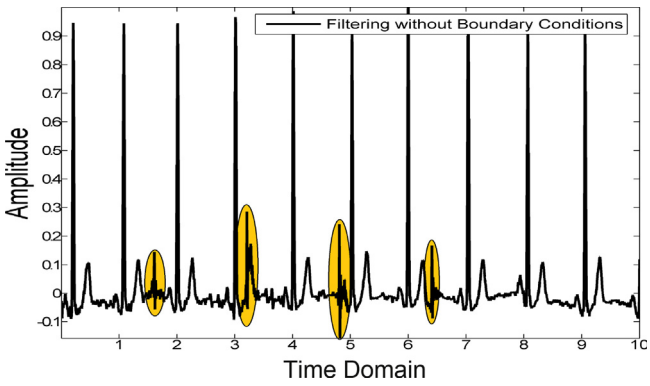

Fig. 3. The results of the proposed scheme without boundary conditions are reported. A ECG signal of 10 s is processed in local way with data blocks of 0.25 s at a time. The figure marks in yellow the distortions on the signal, caused by the incorrect truncation of the scheme between two consecutive elaborated data blocks of the signal. (For interpretation of the references to color in this figure legend, the reader is referred to the web version of the article.)

localized around the connection points between two consecutive acquired portions of the signal.

Here, we provide a methodology that explains how to switch from the forward procedure in (23) to the backward procedure in (24) removing the distortions (as shown in Fig. 3) caused by the truncation errors. It is based on the works of [32,31,22]. We adapt the methodology on boundary conditions to our case, in order to provide a means for the real time computation and visualization of the denoised signal $\vec{s}_h$. To achieve this aim, let $s_0[j], j = 1, \ldots, n$ a part of the signal (supposed with infinite size) as shown in Fig. 4. The aim is to obtain the denoised signal $s_{\tilde{h}}[j]$, from $s_0[j]$, $\forall j = 1, \ldots, n$. In order to apply Eqs. (23) and (24) determined for infinite signals, first, the right border of $\vec{s}_0$ subdomain is virtually extended by adding infinite points, called ghost points, as shown in Fig. 5. Once the grid is ideally extended, later we complete the right hand side of $\vec{s}_0$ on interval $[n, n+eg]$ (with eg an arbitrary number of points) by means of a polynomial which sets to 0 the signal, as also shown in Fig. 5. In our implementation we have chosen a third degree Hermite polynomial q but it is possible to choose every function that goes to a zero value. The constraints on the Hermite polynomial q are the following:

$$\text{if} \quad \frac{s_0[n] - s_0[n-1]}{\tau} \geq 0 \quad \text{then}$$
$$\Rightarrow \quad \begin{cases} q[1] = s_0[n] \\ q'[1] = 0 \end{cases} \quad \text{and} \quad \begin{cases} q[eg] = 0 \\ q'[eg] = 0 \end{cases} \tag{28}$$

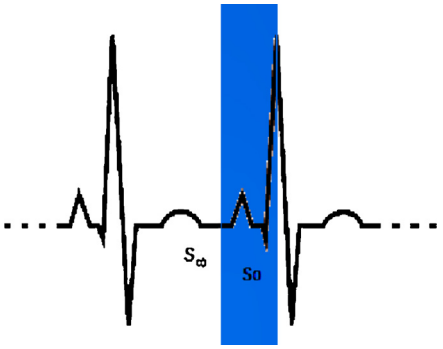

Fig. 4. An infinite ECG signal $\vec{s}_\infty$ and its finite part $\vec{s}_0$, marked in blue. (For interpretation of the references to color in this figure legend, the reader is referred to the web version of the article.)

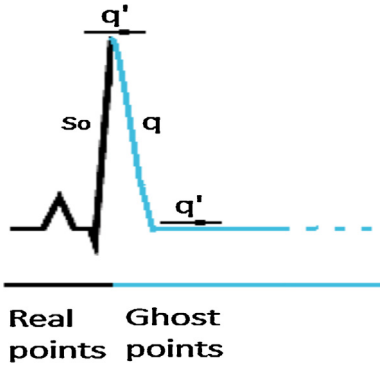

Fig. 5. The extension of the signal $\vec{s}_0$ on the right, adding infinite imaginary points (Ghost points) by means of a Hermite polynomial (blue line) that puts to zero the signal. (For interpretation of the references to color in this figure legend, the reader is referred to the web version of the article.)

otherwise,

$$\text{if} \quad \frac{s_0[n] - s_0[n-1]}{\tau} < 0 \quad \text{then}$$
$$\Rightarrow \begin{cases} q[1] = s_0[n] \\ q'[1] = \dfrac{s_0[n] - s_0[n-1]}{\tau} \end{cases} \quad \text{and} \quad \begin{cases} q[eg] = 0 \\ q'[eg] = 0. \end{cases} \tag{29}$$

Next, we consider the new signal, still indicated with $s_0[j], j = 1, \ldots, +\infty$, defined as:

$$s_0[j] = \begin{cases} s_0[j] = s_0[j], & \forall j = 1, \ldots, n, \\ s_0[j] = q[j-n], & \forall j = n+1, \ldots, n+eg, \\ s_0[j] = 0, & \forall j = n+eg+1, \ldots, +\infty, \end{cases} \tag{30}$$

that extends the previous signal to infinity.

Using these new assumptions and a matrix formulation of the forward procedure (23), the following holds:

$$\begin{pmatrix} p_{\tilde{h}}[j+1] \\ p_{\tilde{h}}[j] \end{pmatrix} = \mathbf{A} \begin{pmatrix} p_{\tilde{h}}[j] \\ p_{\tilde{h}}[j-1] \end{pmatrix}, \quad \text{with} \quad \mathbf{A} = \begin{pmatrix} a_1 & a_2 \\ 1 & 0 \end{pmatrix},$$
$$\forall j \geq n + eg + 2. \tag{31}$$

More generally, by means of the formulation in (31), it is easy to proof that:

$$\begin{pmatrix} p_{\tilde{h}}[j+k] \\ p_{\tilde{h}}[j+k-1] \end{pmatrix} = \mathbf{A}^k \begin{pmatrix} p_{\tilde{h}}[j] \\ p_{\tilde{h}}[j-1] \end{pmatrix} \begin{matrix} \forall j \geq n + eg + 2, \\ \forall k \in \mathbb{N}. \end{matrix} \tag{32}$$

Similarly, placed with $\mathbf{U} = \begin{pmatrix} 1 & 0 \\ 0 & 0 \end{pmatrix}$ and employing a matrix notation for the backward procedure in (24), the following identity holds:

$$\begin{pmatrix} s_{\tilde{h}}[j] \\ s_{\tilde{h}}[j+1] \end{pmatrix} = b_0 \mathbf{U} \begin{pmatrix} p_{\tilde{h}}[j] \\ p_{\tilde{h}}[j-1] \end{pmatrix} + b_1 \mathbf{U}\mathbf{A} \begin{pmatrix} p_{\tilde{h}}[j] \\ p_{\tilde{h}}[j-1] \end{pmatrix}$$
$$+ b_2 \mathbf{U}\mathbf{A}^2 \begin{pmatrix} p_{\tilde{h}}[j] \\ p_{\tilde{h}}[j-1] \end{pmatrix} + \mathbf{A} \begin{pmatrix} s_{\tilde{h}}[j+1] \\ s_{\tilde{h}}[j+2] \end{pmatrix}, \quad \forall j \geq n + eg + 2. \tag{33}$$

Placing with $\mathbf{C} = \mathbf{U}(b_0\mathbf{I} + b_1\mathbf{A} + b_2\mathbf{A}^2)$ and $\mathbf{I} = \begin{pmatrix} 1 & 0 \\ 0 & 1 \end{pmatrix}$ then (33) becomes:

$$\begin{pmatrix} s_{\tilde{h}}[j] \\ s_{\tilde{h}}[j+1] \end{pmatrix} = \mathbf{C} \begin{pmatrix} p_{\tilde{h}}[j] \\ p_{\tilde{h}}[j-1] \end{pmatrix} + \mathbf{A} \begin{pmatrix} s_{\tilde{h}}[j+1] \\ s_{\tilde{h}}[j+2] \end{pmatrix}, \quad \forall j \geq n + eg + 2 \tag{34}$$

from which, for K steps and $\forall j \geq n + eg + 2$, we obtain the following statement:

$$\begin{pmatrix} s_{\tilde{h}}[j] \\ s_{\tilde{h}}[j+1] \end{pmatrix} = \left(\sum_{k=0}^{K-1} \mathbf{A}^k \mathbf{C} \mathbf{A}^k \right) \begin{pmatrix} p_{\tilde{h}}[j] \\ p_{\tilde{h}}[j-1] \end{pmatrix} + \mathbf{A}^K \begin{pmatrix} s_{\tilde{h}}[j+K] \\ s_{\tilde{h}}[j+K+1] \end{pmatrix}. \tag{35}$$

The convergence of the sequence A^k, for $k \to +\infty$ is related to the spectral ray $\rho(A)$ of the matrix A, as stated by Gelfand's formula. It is easy to prove that $\rho(A) < 1$ by means of the a_1 and a_2 values determined in Theorem 3.3. Then we obtain that:

$$\rho(A) = e^{-\sqrt{2}\sigma\tau} < 1 \Rightarrow \lim_{K \to +\infty} \mathbf{A}^K = 0. \tag{36}$$

Then, $\vec{s}_h$ being limited, the equation in (35), for $K \to +\infty$, becomes:

$$\begin{pmatrix} s_{\tilde{h}}[j] \\ s_{\tilde{h}}[j+1] \end{pmatrix} = \left(\sum_{k=0}^{\infty} \mathbf{A}^k \mathbf{C} \mathbf{A}^k \right) \begin{pmatrix} p_{\tilde{h}}[j] \\ p_{\tilde{h}}[j-1] \end{pmatrix}, \quad \forall j \geq n + eg + 2. \tag{37}$$

Placed with:

$$\mathbf{X} = \begin{pmatrix} x_{1,1} & x_{1,2} \\ x_{2,1} & x_{2,2} \end{pmatrix} = \sum_{k=0}^{\infty} \mathbf{A}^k \mathbf{C} \mathbf{A}^k, \tag{38}$$

if it is possible to determine the unknowns $x_{j,k}$, $j, k = 1, 2$, that obviously depend on the filter coefficients b_0, b_1, b_2, a_1 and a_2, then we obtain the initial conditions for the backward process and the problem of the incorrect truncation is eliminated. The matrix $\mathbf{X}$ can be developed as:

$$\mathbf{X} = \mathbf{C} + \mathbf{A} \left(\sum_{k=0}^{\infty} \mathbf{A}^k \mathbf{C} \mathbf{A}^k \right) \mathbf{A} \tag{39}$$

and by the statements (38) and (39), $\mathbf{X}$ results as the unique solution of the matrix equation:

$$\mathbf{X} - \mathbf{A}\mathbf{X}\mathbf{A} = \mathbf{C}. \tag{40}$$

The statement in (40) is equivalent to:

$$\mathbf{A}^{-1}\mathbf{X} - \mathbf{X}\mathbf{A} = \mathbf{E}, \quad \text{with} \quad \mathbf{A}^{-1} = \begin{pmatrix} 0 & 1 \\ \frac{1}{a_2} & -\frac{a_1}{a_2} \end{pmatrix} \quad \text{and} \quad \mathrm{E} = \mathbf{A}^{-1}\mathbf{C}. \tag{41}$$

The matrix equation in (41) can be arranged as the following 4×4 linear system:

$$\begin{pmatrix} a_1 & 1 & 1 & 0 \\ a_2 & 0 & 0 & 1 \\ \frac{1}{a_2} & \frac{a_1 a_2 - a1}{a_2} & 0 & 1 \\ 0 & \frac{1}{a_2} & a_2 & -\frac{a_1}{a_2} \end{pmatrix} \begin{pmatrix} x_{1,1} \\ x_{1,2} \\ x_{2,1} \\ x_{2,2} \end{pmatrix} = \begin{pmatrix} e_{1,1} \\ e_{1,2} \\ e_{2,1} \\ e_{2,2} \end{pmatrix} \tag{42}$$

from which we draw the following solution:

$$\begin{pmatrix} x_{1,1} \\ x_{1,2} \\ x_{2,1} \\ x_{2,2} \end{pmatrix} = \begin{pmatrix} a_1 & 1 & 1 & 0 \\ a_2 & 0 & 0 & 1 \\ \frac{1}{a_2} & \frac{a_1 a_2 - a1}{a_2} & 0 & 1 \\ 0 & \frac{1}{a_2} & a_2 & -\frac{a_1}{a_2} \end{pmatrix}^{-1} \begin{pmatrix} e_{1,1} \\ e_{1,2} \\ e_{2,1} \\ e_{2,2} \end{pmatrix}. \tag{43}$$

The statement in (43) returns the explicit formulation of the $x_{j,k}$, j, $k = 1, 2$ that allows us to obtain suitable boundary conditions for the backward procedure (24). In real applications the one-dimensional grid is extended by adding a few ghost points, typically the 15% of the signal's size n is chosen for the parameter eg. After the application of the filter the ghost points are removed. In Fig. 6, we report the results of the scheme with boundary conditions that remove the distortion effects on the ECG signal of Fig. 3. Remember that these errors were caused by the wrong turning conditions in the problem of the real time processing introduced before. Using Eqs. (23), (24), (37) and (43), we report in Algorithm 2 the numerical scheme to filter the ECG signals in a local way, with the boundary conditions, to avoid the edge effects. The implementation of Algorithm 2 in our software framework allows us now to realize the real time filtering and visualization of the denoised signal by means of the recursive filtering scheme.

4.2. Performance results

In this section, we describe the testing of the scheme, for the removal of baseline drift and power line interference from a noisy ECG, in terms of accuracy and efficiency.

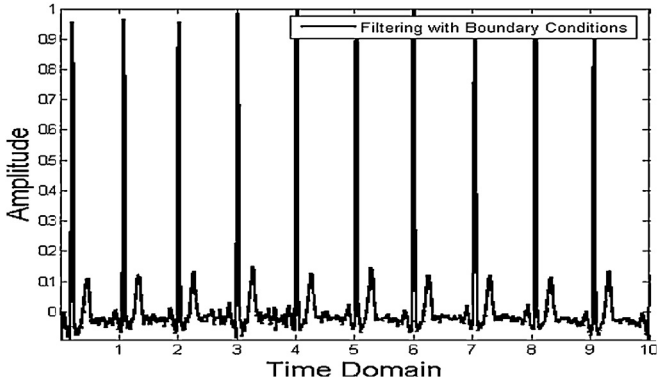

Fig. 6. An ECG signal of 10 s is processed by means of the proposed scheme with the boundary conditions. The signal is filtered in locally way by using data blocks of 0.25 s at a time. The figure shows how, now, the scheme with the boundary conditions added does not cause the distortion effects on the ECG signal.

Algorithm 2. Filtering scheme + boundary conditions

Input: s_0, μ, σ **Output:** $s_{\bar{h}}$
1: Compute b_0, b_1, b_2, a_1, a_2 by means of formulas (25) and (26) % coefficients precomputation
2: Compute $x_{1,1}, x_{1,2}, x_{2,1}, x_{2,2}$ by means of formula (43) % boundary coefficients precomputation
3: for $j = 1, 2, \ldots, N$ % left zero end conditions
4: $p_{\bar{h}}[j - N] := 0$
5: endfor
6: for $j = 1, 2, \ldots, n + eg + 2$ % advancing process
7: $p_{\bar{h}}[j] = b_0 s_0[j] + b_1 s_0[j-1] + b_2 s_0[j-2] + a_1 p_{\bar{h}}[j-1] + a_2 p_{\bar{h}}[j-2]$
8: endfor
9: $s_{\bar{h}}[n + eg + 2] := x_{2,1} p_{\bar{h}}[n + eg + 1] + x_{2,2} p_{\bar{h}}[n + eg]$
10: $s_{\bar{h}}[n + eg + 1] := x_{1,1} p_{\bar{h}}[n + eg + 1] + x_{1,2} p_{\bar{h}}[n + eg]$
11: endfor
12: for $j = n + eg, \ldots, 1$ % backing process
13: $s_{\bar{h}}[j] = b_0 p_{\bar{h}}[j] + b_1 p_{\bar{h}}[j+1] + b_2 p_{\bar{h}}[j+2] + a_1 s_{\bar{h}}[j+1] + a_2 s_{\bar{h}}[j+2]$
14: endfor

Baseline drift is caused by respiration or patient movement which creates problems in the detection of peaks (see Figs. 7 and 9). Due to wandering the T peak could be higher than the R peak and might be detected as an R peak instead. It is normally considered below 1 Hz. Power line interference consists of 60/50 Hz pickup and harmonics and the amplitude is 50% of peak-to-peak ECG amplitude. Some of the common causes of the 50 Hz interferences are reported in [33].

In our experiments, we used data from the Physionet Long-Term ST Database [34]. The Long-Term ST Database contains 86 lengthy ECG recordings of 80 human subjects, chosen to exhibit a variety of events of ST segment changes, including ischemic ST episodes, axis-related non-ischemic ST episodes, episodes of slow ST level drift, and episodes containing mixtures of these phenomena. The database was created to support the development and evaluation of algorithms capable of accurately differentiating ischemic and non-ischemic ST events, and to enable basic research into mechanisms and dynamics of myocardial ischemia. Hence, a pre-processing phase for the removal of the additional artifacts on the ECGs is necessary, in order to enable these algorithms to realize an efficient detection of physiological and pathological events.

The ECG signals used in this work for our experiments last 3600 s and are: s20011, s20021, s20031, s20041, s20051, s20061, s20071, s20081, s20091 and 20101. These recordings were sampled at 250 Hz using 11-bit A/D converters. First, we processed the Physionet recordings (converted to millivolts) with only the synthetic baseline wander noise and then with the baseline wander noise and the power line interference added. We set the baseline wander with a frequency varying from 0.1 to 0.3 Hz and an amplitude varying from 0 to 2500 μV and the power line interference with a frequency varying from 49 to 51 Hz and an amplitude varying from 0 to 500 μV. In particular, in our first tests we compared, in terms of accuracy measurement, the results of the proposed scheme (RF) for the removal of the baseline wander. A very important feature here is that in order to test the RF with the boundary conditions, also for the real time denoising, we processed the whole ECG signal

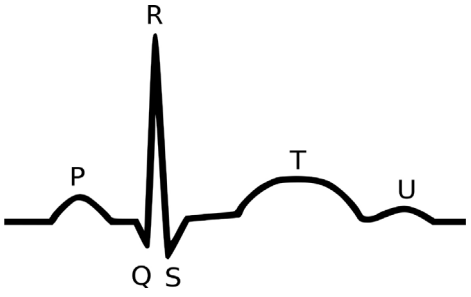

Fig. 7. An example of a standard ECG waveform with its fundamental peaks and waves.

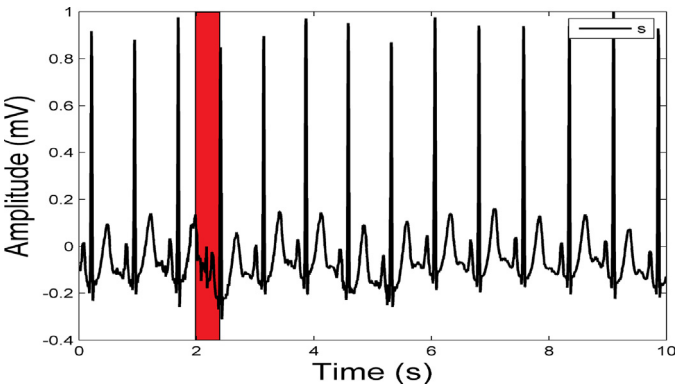

Fig. 8. A part of the signal $\bar{s}$ that contains the first 10 s of ECG s20071.

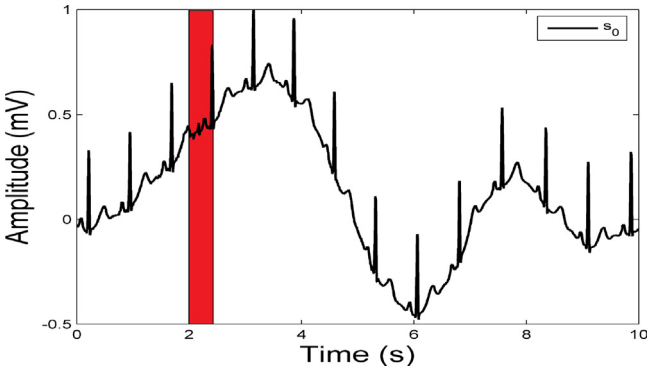

Fig. 9. The noisy signal $\bar{s}_0$, obtained from the signal $\bar{s}$, adding the baseline drift.

partitioning it in 14.400 parts of 0.25 s. We proceeded to compare the accuracy results of the RF, only for the removal of the baseline, to those of methods that exploit the FFT (BPF), including those of a first order zero-phase lowpass filter (LPF) (e.g. [28,6]), of a single stage of median filtering (SMEDF), of a double stage of median filtering (DMEDF) [35,8,36], of a double stage of moving average filtering (DMEAF) [37] and of the Kalman filter (KF) [9].

Let $\bar{s}$ be the true signal s20071m (Fig. 8) and $\bar{s}_0$ the noisy signal (Fig. 9) obtained from s by adding synthetic baseline drift, as described above. We report in Fig. 10 the deinoised signals obtained by the RF filter with $\mu = 0.25$ Hz and $\sigma = 0.9$ Hz. In all figures, the signals were normalized for a better visualization. The first qualitative impression on the denoising and shape preserving is that RF reconstructs quite successfully the signal $\bar{s}$ also in a part of the ECG where there is a pathological event (the red zone in Fig. 10).

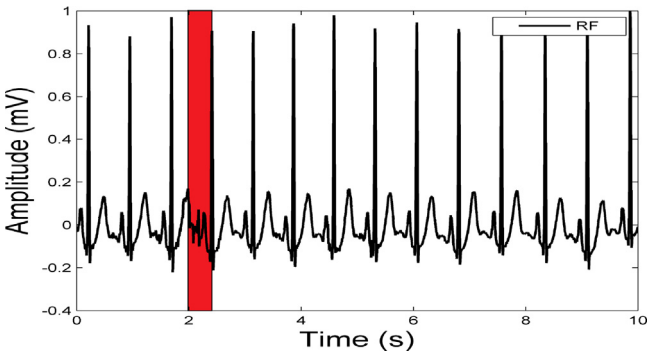

Fig. 10. The denoised signal obtained by means of RF, with $\mu = 0.25$ Hz and $\sigma = 0.9$ Hz. (For interpretation of the references to color in this sentence, the reader is referred to the web version of the article.)

Table 2
Signal-to-noise ratio (SNR) (in decibels).

SNR	LPF	SMEDF	DMEDF	DMEAF	KF	BPF	RF
s20011	16.69	14.06	14.09	17.54	13.73	19.12	19.12
s20021	17.19	16.53	16.59	17.63	15.59	18.92	18.71
s20031	19.35	16.06	16.43	20.19	15.56	22.93	22.19
s20041	3.09	16.06	2.18	3.12	2.92	3.16	3.15
s20051	16.27	12.22	13.27	17.47	12.02	18.22	18.12
s20061	18.43	14.23	14.43	19.43	14.64	21.36	21.19
s20071	17.22	13.33	13.53	17.70	14.99	18.63	18.61
s20081	16.10	13.94	14.25	16.57	14.33	17.42	17.40
s20091	17.21	14.37	14.67	18.09	13.41	19.15	19.04
s20101	18.02	15.49	15.49	18.75	15.24	20.22	20.22

As in [38,39], we quantify the denoising performance in terms of the Signal-to-Noise ratio (SNR) (in decibels):

$$SNR = 10\log_{10}\left(\frac{\sum_{i=1}^{n}(s_0[i]-s[i])^2}{\sum_{i=1}^{n}(s_f[i]-s[i])^2}\right). \quad (44)$$

In (44), $\vec{s}_f$ is one of the denoised signals obtained by means of the filters used and n is the length of $\vec{s}$, $\vec{s}_0$ and $\vec{s}_f$. Here we highlight that we have assumed the Physionet signals $\vec{s}$ to be the actual signals; however, these signals also contain noise, which is neglected by the metric chosen.

In Table 2, we report the SNR measures of the ECGs chosen in the paper, varying the filters considered.

First of all, we can observe from Table 2, that the most accurate filter is, in any case, BPF (based on the FFT method), with in second position RF and in third position the DMEAF. We highlight that the tests on the accuracy of the RF were performed using the boundary conditions derived above in order to allow the real time processing.

As a second step, we added to the considered ECG recordings a combination of synthetic baseline drift and synthetic power line interference as described before. This time we compared the accuracy results of RF to those of a method that again exploits the FFT method (BPF), of zero-phase low pass and high pass filters (Z(L/H)PF) (e.g. [28,6]) belonging to the group of Finite Impulsive Response filters (e.g. [13]), of the Wiener filter (WF) (e.g. [10]) and of a filter based on wavelet decomposition (WDF) (e.g. [12]). In Fig. 11, we report the noisy signal, obtained by $\vec{s}$, adding synthetic baseline drift and power line interference, as described above. In Fig. 12, we show the denoised signal obtained by means of RF applied two times, the first time with $\mu = 0.25$ Hz and $\sigma = 0.9$ Hz for the removal of the baseline wander and the second time with $\mu = 50$ Hz and $\sigma = 15$ Hz for the removal of the power line interference. In Table 3, we give the respective SNR measurements for the considered filters.

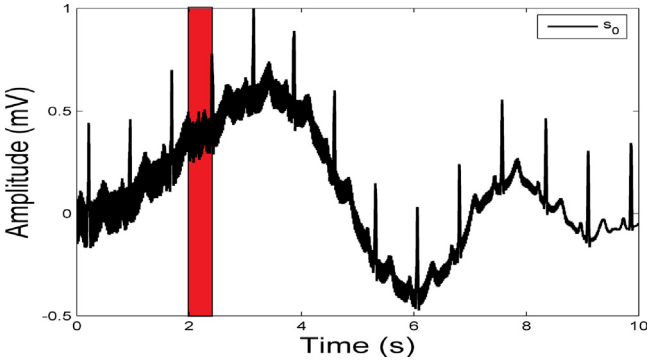

Fig. 11. The noisy signal $\vec{s}_0$, obtained from the signal $\vec{s}$, adding baseline drift and power line interference.

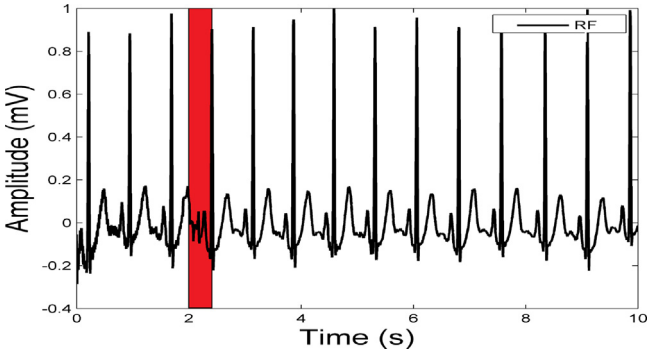

Fig. 12. The denoised signal obtained after a serial application of RF, first with $\mu = 0.25$ Hz and $\sigma = 0.9$ Hz and secondly with $\mu = 50$ Hz and $\sigma = 15$ Hz.

Table 3
Signal-to-noise ratio (SNR) (in decibels).

SNR	BPF	Z(L/H)PF	WF	WDF	RF
s20011	18.59	17.13	16.68	17.54	18.48
s20021	17.47	15.88	17.12	15.16	17.21
s20031	21.32	17.98	21.22	17.98	21.28
s20041	2.74	2.63	2.61	2.65	2.70
s20051	17.46	14.97	17.24	15.68	17.38
s20061	20.61	17.70	20.34	17.01	20.43
s20071	17.93	16.31	17.71	15.79	17.88
s20081	16.81	15.72	16.25	15.07	16.74
s20091	18.37	16.15	18.17	15.86	18.31
s20101	19.47	17.34	18.37	16.52	19.38

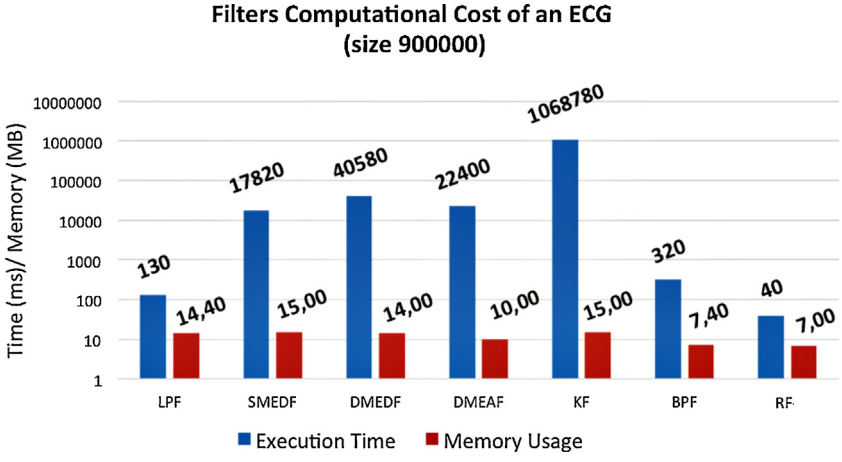

Fig. 13. The computational cost (execution time and memory usage) of BPF, DMEDF, DMEAF, KF, BPF and RF to denoise an ECG (s20011) with a size n of 900 000 samples.

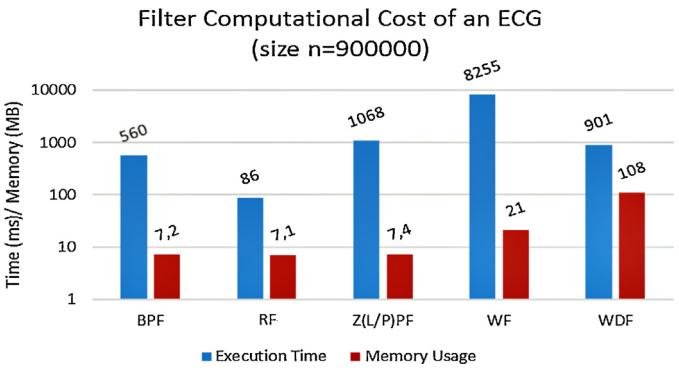

Fig. 14. The computational cost (execution time and memory usage) of BPF, Z(L/H)PF, WF and WDF and RF to denoise an ECG (s20011) with a size n of 900 000 samples.

Once again, we recall that for RF the time domain was divided into subdomains and boundary conditions were applied. In Tables 2 and 3 we show that the accuracy of our scheme, in terms of SNR measurements, is comparable with that of the other filters and is the best in some cases. To emphasize the contribution of this work, in relation to the computational cost of the new algorithm, we show respectively, in Figs. 13 and 14, the average results of the first and second experiment, in terms of execution time and memory usage, of RF and of other examined filters, for the denoising of ECG s20071 (size $n = 900\,000$). The experiments were carried out using an Asus CPU Intel(R) Core(TM) i7-4510U CPU 2.00 GHZ −2.60 GHZ, RAM 6 GB. Figs. 13 and 14 show that RF and BPF have the lowest time consumption and use the smallest amount of memory.

Taking into consideration the SNR measurements in Tables 2 and 3 and the computational cost tests in Figs. 13 and 14; RF has the possibility of an easy implementation also on architectures with a limited capacity in terms of computing and memory, such as mobile devices.

Finally, from a medical point of view, the shape parameters preserving of a filter is a very important issue. To ensure that our numerical scheme had this feature, we used *KubiosHRV*, a software for heart rate variability (HRV) computing. (for an excellent tutorial see [40]). For all ECGs tested from Physionet database, we checked that: after the application of RF on the synthetic noisy signals, the peak to peak distance (RR) and the heart rate (HR) of the denoised signals were equal to the original signals. In Fig. 15 we report the histograms of the main ECG (s20071m) parameters: the RR and HR of the noisy signal s_0, the actual signal s and the denoised signal $s_{\tilde{h}}$ obtained by means of *KubiosHRV*. We can observe in Fig. 15 that starting from the noisy signal $\vec{s}_0$, after the application of the filter, all the biomedical parameters of the actual signal $\vec{s}$ and the denoised signal $\vec{s}_{\tilde{h}}$ are preserved.

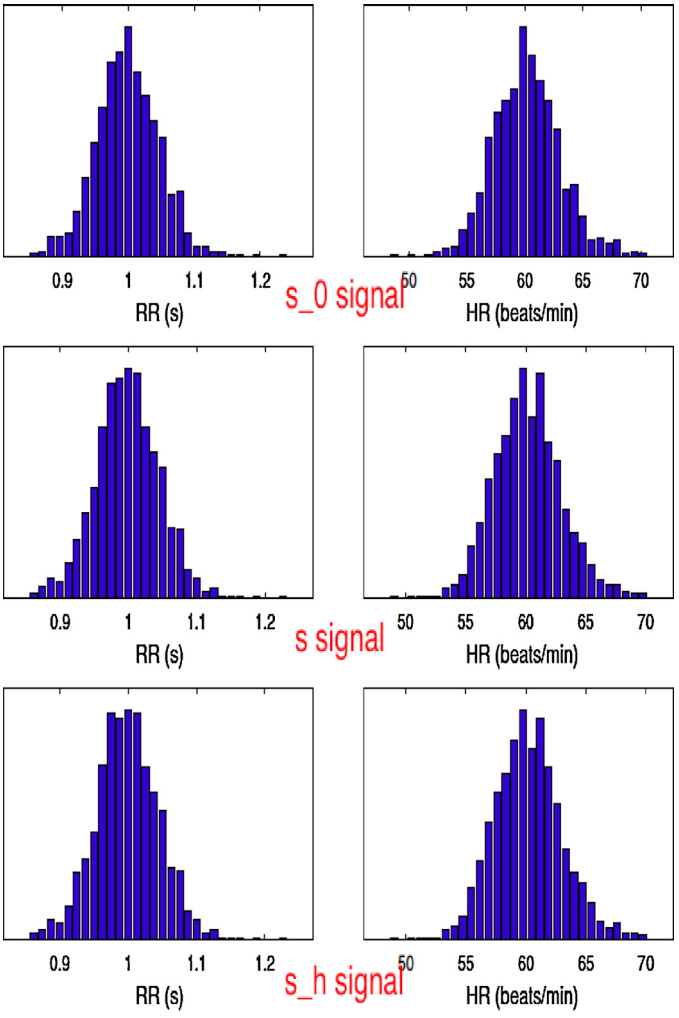

Fig. 15. Peak to peak distance (RR) and heart rate (HR) parameters for $\vec{s}$, $\vec{s}_0$ and $\vec{s}_h$ signals.

5. Conclusions

In this paper, we have described the implementation of an algorithm (RF) for ECG Signal processing applicable in the context of real-time health monitoring, where signal processing efficiency is strictly demanded.

Numerical experiments on some ECGs from the Physionet database have demonstrated that our RF can significantly reduce the total computational cost of the denoising for some kinds of noise such as baseline wander and powerline interference, compared to other efficient filters, while maintaining the same level of accuracy and using only a few code lines.

In the work, we have provided the theoretical development of the new algorithm, based on the studies of [19,20,30], where the authors formulated their scheme in the context of signal processing and other research fields to eliminate high frequency noise. We have adapted this for ECG signal denoising, providing a description of the process to obtain the RF coefficients for the main artifacts of ECG recordings. In addition, we have also provided the boundary conditions for local denoising that allow the visualization of the denoised signal in real time.

RF is fast and accurate as shown by the numerical experiments. For those reason, in general, it is possible to implement RF also on architectures with a limited capacity in terms of computing and memory, for example mobile devices.

Acknowledgment

The authors would like to acknowledge the project "*SmartHealth*2 . 0″ −− *PON*04*A*2 _ *C* for its support of this work.

Appendix A.

Proof of Proposition 3.2.. The difference between the convolutions s_h and $s_{\tilde{h}}$ is:

$$s_h - s_{\tilde{h}} = h \otimes s_0 - \tilde{h} \otimes s_0 = (h - \tilde{h}) \otimes s_0. \tag{45}$$

Hence, the following relationship holds:

$$\|s_h - s_{\tilde{h}}\|_2 = \|(h - \tilde{h}) \otimes s_0\|_2. \tag{46}$$

The Cauchy–Schwarz inequality, applied to the right-hand side in (46), gives the following inequality:

$$\|s_h - s_{\tilde{h}}\|_2 \leq \|h - \tilde{h}\|_2 \|s_0\|_2. \tag{47}$$

For the distance between the functions h and $\tilde{H}$, using the Plancherel theorem in (5) and the hypothesis that $0 \leq H, \tilde{H} \leq 1$, it holds that:

$$\begin{aligned} \|h - \tilde{h}\|_2^2 &= \|H - \tilde{H}\|_2^2 \\ &= \int_{-\infty}^{+\infty} |H(\omega) - \tilde{H}(\omega)|^2 \, d\omega \leq \int_{-\infty}^{+\infty} |H(\omega) - \tilde{H}(\omega)| \, d\omega. \end{aligned} \tag{48}$$

By means of the integral's additivity and the symmetry of H and $\tilde{H}$, with respect to μ, the right hand side term of (48) becomes:

$$\begin{aligned} &2 \int_{-\infty}^{+\mu-\sigma} |H(\omega) - \tilde{H}(\omega)| \, d\omega + \int_{\mu-\sigma}^{\mu+\sigma} |H(\omega) - \tilde{H}(\omega)| \, d\omega \\ &= 2 \int_{-\infty}^{\mu-\sigma} \left[1 - \frac{(\omega-\mu)^2}{2\sigma^2 + (\omega-\mu)^2} \right] d\omega \\ &\quad + \int_{\mu-\sigma}^{\mu+\sigma} \left[\frac{(\omega-\mu)^2}{2\sigma^2 + (\omega-\mu)^2} \right] d\omega = 2 \left[\sqrt{2}\sigma \arctan\left(\frac{\omega-\mu}{\sqrt{2}\sigma} \right) \right]_{-\infty}^{\mu-\sigma} \\ &\quad + \left[\omega - \sqrt{2}\sigma \arctan\left(\frac{\omega-\mu}{\sqrt{2}\sigma} \right) \right]_{\mu-\sigma}^{\mu+\sigma} \\ &= \left(2 + \pi\sqrt{2} - 4\sqrt{2} \arctan\left(\frac{1}{\sqrt{2}} \right) \right) \sigma. \end{aligned} \tag{49}$$

Hence from (48) and (49), for $\|h - \tilde{h}\|_2$ it holds that:

$$\|h - \tilde{h}\|_2 \leq \left(\left(2 + \pi\sqrt{2} - 4\sqrt{2} \arctan\left(\frac{1}{\sqrt{2}} \right) \right) \sigma \right)^{1/2} = \mathcal{O}(\sqrt{\sigma}). \tag{50}$$

Lastly, by means of (50) and (47), we reach the thesis in (15).□

Proof of Theorem 3.3.. Considering the continuous functions $\tilde{h}_l$ and $\tilde{h}_r$ as in (13), placed with $s = i\omega$, we obtain the equivalent Laplace Transforms:

$$\tilde{H}_l(s) = \frac{s - i\mu}{s + (\sqrt{2}\sigma - i\mu)}, \qquad \tilde{H}_r(-s) = \frac{-s + i\mu}{-s + (\sqrt{2}\sigma + i\mu)}. \tag{51}$$

Applying to $\tilde{H}_r(-s)$ the ZPM, as described at the beginning of this section, we obtain that:

$$\begin{cases} -s + i\mu = 0 \overset{ZPM}{\Rightarrow} 1 - 2\cos(\mu\tau)z^{-1} + z^{-2} = 0, \\ -s + (\sqrt{2}\sigma + i\mu) = 0 \overset{ZPM}{\Rightarrow} 1 - 2e^{-\sqrt{2}\sigma\tau}\cos(\mu\tau)z^{-1} + e^{-2\sqrt{2}\sigma\tau}z^{-2} = 0. \end{cases} \tag{52}$$

Hence $\tilde{H}_r(-s)$ can be rewritten in the z variable as:

$$\tilde{H}_r(-z) = \frac{1 - 2\cos(\mu\tau)z^{-1} + z^{-2}}{1 - 2e^{-\sqrt{2}\sigma\tau}\cos(\mu\tau)z^{-1} + e^{-2\sqrt{2}\sigma\tau}z^{-2}} \tag{53}$$

and represents the $\tilde{H}_r(-i\omega)$ discretization of step τ. In the same way, applying ZPM to $\tilde{H}_l(s)$, we obtain that:

$$\begin{cases} s - i\mu = 0 \overset{ZPM}{\Rightarrow} 1 - 2\cos(\mu\tau)z + z^2 = 0, \\ s + (\sqrt{2}\sigma - i\mu) = 0 \overset{ZPM}{\Rightarrow} 1 - 2e^{-\sqrt{2}\sigma\tau}\cos(\mu\tau)z + e^{-2\sqrt{2}\sigma\tau}z^2 = 0. \end{cases} \tag{54}$$

Hence $\tilde{H}_l(s)$ can be rewritten in the z variable as:

$$\tilde{H}_l(z) = \frac{1 - 2\cos(\mu\tau)z + z^2}{1 - 2e^{-\sqrt{2}\sigma\tau}\cos(\mu\tau)z + e^{-2\sqrt{2}\sigma\tau}z^2} \tag{55}$$

and represents the $\tilde{H}_r(i\omega)$ discretization of step τ.

Hence, by means of ZPM, we derive the $\mathcal{Z}$-Transform of $\tilde{s}_{\tilde{h}}$ (e.g. [28]):

$$S_{\tilde{h}}(z) = \tilde{H}_l(z) \cdot \tilde{H}_r(-z) \cdot S_0(z). \tag{56}$$

The function $S_{\tilde{h}}(z)$ can be rewritten as:

$$\begin{cases} P_{\tilde{h}}(z) = \tilde{H}_r(-z) \cdot S_0(z), \\ S_{\tilde{h}}(z) = \tilde{H}_l(z) \cdot P_{\tilde{h}}(z); \end{cases} \tag{57}$$

and in accordance with to the statements (53) and (55), (57) is equivalent to:

$$\begin{cases} (1 - 2e^{-\sqrt{2}\sigma\tau}\cos(\mu\tau)z^{-1} + e^{-2\sqrt{2}\sigma\tau}z^{-2})P_{\tilde{h}}(z) = (1 - 2\cos(\mu\tau)z^{-1} + z^{-2})S_0(z), \\ (1 - 2e^{-\sqrt{2}\sigma\tau}\cos(\mu\tau)z + e^{-2\sqrt{2}\sigma\tau}z^2)S_{\tilde{h}}(z) = (1 - 2\cos(\mu\tau)z + z^2)P_{\tilde{h}}(z). \end{cases} \tag{58}$$

Antitransforming, by means of the $\mathcal{Z}^{-1}$ transformation, the previous equations in (58) and exploiting the theorem of the delay (e.g. [28]), we obtain the forward and backward difference scheme in (23) and (24).

Using the equations in (58), it is easy to verify that: $b_0 = 1$, $b_1 = -2\cos(\mu\tau)$, $b_2 = 1$, $a_1 = 2e^{-\sqrt{2}\sigma\tau}\cos(\mu\tau)$ and $a_2 = -e^{-2\cdot\sqrt{2}\sigma\tau}$. Hence we obtain the thesis.□

Appendix B. Supplementary data

Supplementary data associated with this article can be found, in the online version, at http://dx.doi.org/10.1016/j.bspc.2016.02.007.

References

[1] R.E. Kleiger, P.K. Stein, J.T. Bigger, Heart rate variability: measurement and clinical utility, Ann. Noninvasive Electrocardiol. 10 (1) (2005) 88–101.
[2] C. Lee, Y. Zhang, Reduction of motion artifacts from photoplethysmographic recordings using a wavelet denoising approach, in: Biomedical Engineering, 2003. IEEE EMBS Asian-Pacific Conference on, IEEE, 2003, pp. 194–195.
[3] B. Chandrakar, O. Yadav, V. Chandra, A survey of noise removal techniques for ECG signals, Int. J. Adv. Res. Comput. Commun. Eng. 2 (3) (2013) 1354–1357.
[4] G.M. Friesen, T.C. Jannett, M.A. Jadallah, S.L. Yates, S.R. Quint, H.T. Nagle, A comparison of the noise sensitivity of nine QRS detection algorithms, IEEE Trans. Biomed. Eng. 37 (1) (1990) 85–98.
[5] J. Sahambi, S. Tandon, R. Bhatt, Quantitative analysis of errors due to power-line interference and base-line drift in detection of onsets and offsets in ECG using wavelets, Med. Biol. Eng. Comput. 35 (6) (1997) 747–751.
[6] I. Christov, I.K. Daskalov, Filtering of electromyogram artifacts from the electrocardiogram, Med. Eng. Phys. 21 (10) (1999) 731–736.
[7] N. Thakor, Y.-S. Zhu, Applications of adaptive filtering to ECG analysis: noise cancellation and arrhythmia detection, IEEE Trans. Biomed. Eng. 38 (8) (1991) 785–794.
[8] P. Laguna, R. Jane, O. Meste, P.W. Poon, P. Caminal, H. Rix, N.V. Thakor, Adaptive filter for event-related bioelectric signals using an impulse correlated reference input: comparison with signal averaging techniques, IEEE Trans. Biomed. Eng. 39 (10) (1992) 1032–1044.
[9] R. Sameni, M. Shamsollahi, C. Jutten, Filtering electrocardiogram signals using the extended Kalman filter, in: Engineering in Medicine and Biology Society, 2005. IEEE-EMBS 2005. 27th Annual International Conference of the, 2005, pp. 5639–5642.
[10] K.-M. Chang, S.-H. Liu, Gaussian noise filtering from ECG by wiener filter and ensemble empirical mode decomposition, J. Signal Process. Syst. 64 (2) (2011) 249–264.
[11] M. Blanco-Velasco, B. Weng, K.E. Barner, ECG signal denoising and baseline wander correction based on the empirical mode decomposition, Comput. Biol. Med. 38 (1) (2008) 1–13.
[12] S. Poornachandra, Wavelet-based denoising using subband dependent threshold for ECG signals, Dig. Signal Process. 18 (1) (2008) 49–55.

[13] S.L. Joshi, R.A. Vatti, R.V. Tornekar, A survey on ECG signal denoising techniques, in: Communication Systems and Network Technologies (CSNT), 2013 International Conference on, IEEE, 2013, pp. 60–64.
[14] B.H. Tracey, E.L. Miller, Nonlocal means denoising of ECG signals, IEEE Trans. Biomed. Eng. 59 (9) (2012) 2383–2386.
[15] D.M. Malvey, D.J. Slovensky, MHealth: Transforming Healthcare, Springer, 2014.
[16] J. Mattingley, S. Boyd, Real-time convex optimization in signal processing, IEEE Signal Process. Mag. 27 (3) (2010) 50–61.
[17] S.-W. Chen, H.-C. Chen, H.-L. Chan, A real-time QRS detection method based on moving-averaging incorporating with wavelet denoising, Comput. Methods Programs Biomed. 82 (3) (2006) 187–195.
[18] L.C. Parra, C.D. Spence, A.D. Gerson, P. Sajda, Response error correction – a demonstration of improved human–machine performance using real-time EEG monitoring, IEEE Trans. Neural Syst. Rehabil. Eng. 11 (2) (2003) 173–177.
[19] I.T. Young, L.J. Van Vliet, Recursive implementation of the Gaussian filter, Signal Process. 44 (2) (1995) 139–151.
[20] L.J. Van Vliet, I.T. Young, P.W. Verbeek, Recursive Gaussian derivative filters, in: Pattern Recognition, 1998. Proceedings. Fourteenth International Conference on. vol. 1, IEEE, 1998, pp. 509–514.
[21] S. Cuomo, R. Farina, A. Galletti, L. Marcellino, An error estimate of Gaussian recursive filter in 3Dvar problem, in: Proceedings of the 2014 Federated Conference on Computer Science and Information Systems, vol. 2, Annals of Computer Science and Information Systems, IEEE, 2014.
[22] S. Cuomo, R. Farina, A. Galletti, L. Marcellino, A K-iterated scheme for the first-order Gaussian recursive filter with boundary conditions., in: Proceedings of the 2015 Federated Conference on Computer Science and Information Systems, vol. 5, Annals of Computer Science and Information Systems, IEEE, 2015.
[23] R. Farina, S. Dobricic, S. Cuomo, Some numerical enhancements in a data assimilation scheme, in: 11th International Conference of Numerical Analysis and Applied Mathematics 2013: ICNAAM 2013, AIP Publishing, 2013, pp. 2369–2372.
[24] R. Farina, S. Dobricic, A. Storto, S. Masina, S. Cuomo, A revised scheme to compute horizontal covariances in an oceanographic 3D-VAR assimilation system, J. Comput. Phys. (2015), http://dx.doi.org/10.1016/j.jcp.2015.01.003, ISSN 0021-9991.
[25] S. Cuomo, A. Galletti, R. Farina, G. De Pietro, G. Sannino, A framework for ECG denoising for mobile devices, in: Proceedings of the 8th ACM International Conference on PErvasive Technologies Related to Assistive Environments, ACM, 2015, p. 48.
[26] S. Cuomo, G. De Pietro, R. Farina, A. Galletti, G. Sannino, A novel $O(n)$ numerical scheme for ECG signal denoising, Procedia Comput. Sci. 51 (2015) 775–784.
[27] A. Buades, B. Coll, J.-M. Morel, A non-local algorithm for image denoising, in: Computer Vision and Pattern Recognition, 2005. CVPR 2005. IEEE Computer Society Conference on, vol. 2, IEEE, 2005, pp. 60–65.
[28] A.V. Oppenheim, A.S. Willsky, S.H. Nawab, Signals and Systems, vol. 2, Prentice-Hall, Englewood Cliffs, NJ, 1983.
[29] I. Christov, I. Dotsinsky, I. Daskalov, High-pass filtering of ECG signals using QRS elimination, Med. Biol. Eng. Comput. 30 (2) (1992) 253–256.
[30] R.J. Purser, W.-S. Wu, D.F. Parrish, N.M. Roberts, Numerical aspects of the application of recursive filters to variational statistical analysis. Part I: Spatially homogeneous and isotropic Gaussian covariances, Mon. Weather Rev. 131 (8) (2003) 1524–1535.
[31] B. Triggs, M. Sdika, Boundary conditions for Young–van Vliet recursive filtering, IEEE Trans. Signal Process. 54 (6) (2006) 2365–2367.
[32] S. Dobricic, N. Pinardi, An oceanographic three-dimensional variational data assimilation scheme, Ocean Model. 22 (3) (2008) 89–105.
[33] G. Garg, S. Gupta, V. Singh, J. Gupta, A. Mittal, Identification of optimal wavelet-based algorithm for removal of power line interferences in ECG signals, in: Power Electronics (IICPE), 2010 India International Conference on, IEEE, 2011, pp. 1–5.
[34] A.L. Goldberger, L.A. Amaral, L. Glass, J.M. Hausdorff, P.C. Ivanov, R.G. Mark, J.E. Mietus, G.B. Moody, C.-K. Peng, H.E. Stanley, Physiobank, physiotoolkit, and physionet components of a new research resource for complex physiologic signals, Circulation 101 (23) (2000) e215–e220.
[35] P. Strumillo, Nested median filtering for detecting t-wave offset in ECGs, Electron. Lett. 38 (14) (2002) 682–683.
[36] P. De Chazal, M. O'Dwyer, R.B. Reilly, Automatic classification of heartbeats using ECG morphology and heartbeat interval features, IEEE Trans. Biomed. Eng. 51 (7) (2004) 1196–1206.
[37] H. Chen, A moving average based filtering system with its application to real-time QRS detection, in: Computers in Cardiology, IEEE, 2003, pp. 585–588.
[38] M.A. Kabir, C. Shahnaz, Denoising of ECG signals based on noise reduction algorithms in EMD and wavelet domains, Biomed. Signal Process. Control 7 (5) (2012) 481–489.
[39] B.H. Tracey, E.L. Miller, Nonlocal means denoising of ECG signals, IEEE Trans. Biomed. Eng. 59 (9) (2012) 2383–2386.
[40] M.P. Tarvainen, J.-P. Niskanen, J. Lipponen, P. Ranta-Aho, P. Karjalainen, Kubios HRV – a software for advanced heart rate variability analysis, in: 4th European Conference of the International Federation for Medical and Biological Engineering, Springer, 2009, pp. 1022–1025.